Functional Comparison of the NAD Binding Cleft of ADP-Ribosylating Toxins†

Katherine M. Dolan,‡ George Lindenmayer,§ and Joan C. Olson*,‡

Departments of Pathology and Laboratory Medicine and of Cell and Molecular Pharmacology and Experimental Therapeutics, Medical University of South Carolina, Charleston, South Carolina 29425

Received December 13, 1999; Revised Manuscript Received March 15, 2000

ABSTRACT: Although a common core structure forms the active site of ADP-ribosylating (ADPRT) toxins, the limited-sequence homology within this region suggests that different mechanisms are being used by toxins to perform their shared function. To explain differences in their mechanisms of NAD binding and hydrolysis, the functional interrelationship of residues predicted to perform similar functions in the β3-strand of the NAD binding cleft of different ADPRT toxins was compared. Replacing Tyr54 in the A-subunit of diphtheria toxin (DTA) with a serine, its functional homologue in cholera toxin (CT), resulted in the loss of catalytic function but not NAD binding. The catalytic role of the aromatic portion of Tyr54 in the ADPRT reaction was confirmed by the ability of a Tyr54-to-phenylalanine DTA mutant to retain ADPRT activity. In reciprocal studies, positioning a tyrosine in the β3-strand of the A1-subunit of CT (CTA1) caused both loss of function and altered structure. The restricted flexibility of the CTA1 active site relative to function became evident upon the loss of ADPRT activity when a conservative Val60-to-leucine mutation was performed. We conclude from our studies that DT and CT maintain a similar mechanism of NAD binding but differ in their mechanisms of NAD hydrolysis. The aromatic moiety at position 54 in DT is integral to NAD hydrolysis, while NAD hydrolysis in CT appears highly dependent on the precise positioning of specific residues within the β3-strand of the active-site cleft.

Toxins play major roles in the virulence of a large number of bacterial pathogens. Although the effects of bacterial toxins can be diverse, many have been found to have a common ADP-ribosyltransferase (ADPRT)[1] mechanism of action. In this complex enzymatic reaction, NAD is split and the ADP-ribose moiety is transferred to a eukaryotic protein substrate, altering the function of that protein. The diverse effects of the different ADP-ribosylating toxins reflect the substrate specificity or the amino acid residue modified by the toxin.

Although ADP-ribosylating toxins have been extensively studied, the precise mechanism of the ADPRT reaction remains unknown. Crystallographic studies have identified a common core-fold in ADP-ribosylating toxins which is composed of ~100 amino acids and includes the NAD binding/hydrolysis active site (*1, 2*). Two antiparallel β-sheets, two α-helices, and a glutamic acid residue come together to form the NAD-hydrolysis cleft. Only limited sequence homology is observed among the different ADP-ribosylating toxins when amino acid residues that form the common enzymatic core are structurally aligned. The sequence variability associated with these active-site regions suggests that mechanisms of NAD binding and hydrolysis are different among the toxins.

Biochemical and mutagenesis studies (summarized in ref *3*), in combination with DT−NAD and exotoxin A−NAD analogue cocrystallization studies (*2, 4*), have identified specific residues in the active site of ADP-ribosylating toxins associated with the enzymatic reaction. An arginine or histidine residue within a β-strand that forms one side of the NAD binding cleft is predicted to play a role in binding the ribose portion of NAD and in maintaining the integrity of the cleft. Tyrosine or serine residues within a β-strand and an α-helix that form the other side of the cleft appear to facilitate the stacking of the nicotinamide portion of NAD into the cleft. Specific residues in this region also contribute to the integrity of the cleft. Both functional and structural data support the involvement of the conserved glutamic acid residue in the catalysis of the ADPRT reaction. Residues involved in the recognition of the specific eukaryotic target substrates of toxins remain unknown.

Studies described in this paper were designed to gain insight into differences in the mechanism of NAD binding and hydrolysis by ADP-ribosylating toxins. The focus of these studies was a β-strand (referred to as the β3-strand) which represents the most highly conserved contiguous sequence within the NAD binding/hydrolysis cleft and which is identified by the consensus sequence F/Y·X·S·T·X (with X representing a more variable residue). Variations in this

† This work was supported by Public Health Service Grant AI30558 from the National Institutes of Allergy and Infectious Diseases and by the Medical University of South Carolina Institutional Research Funds.

* To whom correspondence should be addressed. Department of Pathology and Laboratory Medicine, Medical University of South Carolina, 165 Ashley Ave., Suite 309, P.O. Box 250908, Charleston, SC 29425. Phone: 843-792-7761. Fax: 843-792-4157. E-Mail: olsonj@musc.edu.

‡ Department of Pathology and Laboratory Medicine.

§ Department of Cell and Molecular Pharmacology and Experimental Therapeutics.

[1] Abbreviations: ADPRT, ADP-ribosyltransferase; ARF, ADP-ribosylating factor; BSA, bovine serum albumin; CT, cholera toxin; CTA1, cloned enzymatically active portion (residues 1−192) of CT; DT, diphtheria toxin; DTA, cloned enzymatically active portion (residues 1−193) of DT; EF-2, elongation factor 2; ETA, *Pseudomonas aeruginosa* exotoxin A; ExoS, *P. aeruginosa* exoenzyme S; LT, *Escherichia coli* heat-labile toxin; NAD-GH, NAD-glycohydrolase; TCA, trichloracetic acid.

10.1021/bi992856q CCC: $19.00
Published on Web 06/23/2000

sequence among different toxins, coupled with molecular modeling studies, have led to the division of ADP-ribosylating proteins into two groups: (1) the CT group, which includes the majority of the mono-ADPRTs, and (2) the DT group, which includes ETA and eukaryotic poly-ADP-ribosylpolymerases (*5*). These two groups are predicted to have different mechanisms of NAD binding.

The premise of our studies was that functional differences in the mechanism of NAD binding and hydrolysis of the two groups of toxins could be elucidated by exchanging residues predicted to perform similar functions within the β3-strand of their NAD binding clefts. The results from these studies support that, unlike previous predictions, the sequence diversity within the β3-strand of DT and CT groups does not reflect differences in their mechanism of NAD binding but, rather, reflects their acquisition of different mechanisms of NAD hydrolysis.

EXPERIMENTAL PROCEDURES

Materials. Oligonucleotides were synthesized by the Biotechnology Resource Laboratory at the Medical University of South Carolina. CT and DT were purchased from List Biological Laboratories, Inc. (Campbell, CA). Restriction enzymes and ligase were purchased from New England BioLabs, Inc. (Beverly, MA). Radionucleotides [*adenine*-^{14}C]NAD (241 Ci/mol), [*carbonyl*-^{14}C]NAD (53 Ci/mol), and [^{35}S]dATP (>1000 Ci/mol) were purchased from Amersham Life Sciences (Arlington Heights, IL). All other reagents were of analytical grade and purchased from commercial sources.

Cloning the CT A1-Subunit (CTA1), the DT A-Subunit (DTA), and Exoenzyme S (ExoS) for Mutagenesis. Plasmid pRIT10481 (ATCC #39053), plasmid pDgamma2 (ATCC #67011), and pUC*exoS* (a gift from Dr. Dara Frank, Medical College of Wisconsin, Milwaukee, WI) (*6*) were used as the target DNA for PCR amplification of the CTA1, DTA, and ExoS genes, respectively. Oligonucleotides used for amplification of the CTA1 and the DTA genes incorporated an *Nde*I or *Pst*I site in the forward or reverse primers, respectively, to facilitate directional cloning and in-frame expression of the gene products in the site-directed mutagenesis vector pALTER-*Ex*2 (Promega, Madison, WI). The forward primer for CTA1, 5′-GGCGCATATGAATGATGATAAGTTATATCGGGC-3′, omitted the CTA signal sequence, and the reverse primer, 5′-CCGCCTGCAG**TTA**TCC**TCA**CGATGATCTTGGAGCATTC-3′, included translational stop codons. (Restriction sites are underlined, and translation stop codons are in bold). The forward primer for DTA, 5′-GGCACATATGGGCGCTGATGATGTTGTTGATTC-3′, also omitted the DTA signal sequence, and the reverse primer 5′-CTCGCTGCAG**TTA**TCC**TCA**TCGCCTGACACGATTTCCTGCACA 3′, included two translational stop codons. ExoS was cloned into pET-15b (Novagen, Madison, WI) using an *Nde*I site incorporated into the forward primer and a reverse primer that included a *Bam*HI site downstream of the cloned ExoS structural gene. The forward and reverse primers for ExoS were 5′-GAGTCCATATGGTATCGGCCGACAAGGCGCTG-3′ and 5′-GCATGGATCCGCTGCCGAGCCAAGAATC-3′, respectively. PCR reactions contained 100 ng of plasmid DNA, 1 μg of each of the primers, 200 μM each dNTP, and 10 units of *Taq* DNA polymerase (Perkin-Elmer, Branchburg, NJ). The mixture was subjected to 25 cycles at the following conditions: 94 °C for 30 s, followed by a 2-min cycle of annealing, and extension at 65 °C. The resultant products were digested with the appropriate enzymes and ligated into either pALTER-*Ex*2 or pET-15b. Products of ligation reactions were transformed into *Escherichia coli*, strain JM109 or BL21, by electroporation and plated onto selective medium. Clones were subjected to two rounds of antibiotic selection and colony purification prior to plasmid isolation. The correct size and orientation of the CTA1, DTA, and ExoS genes were determined by restriction digestions, and dideoxy sequencing was used to confirm that no anomalies had occurred within the gene during amplification (Sequenase, U.S. Biochemical Corp., Cleveland, OH).

Site-Directed Mutagenesis. Mutagenesis was performed using either the Altered Sites II-*Ex*2 in vitro Mutagenesis System (Promega, Madison, WI) or the QuikChange Site-Directed Mutagenesis Kit (Stategene, La Jolla, CA), according to the manufacturer's specifications. Oligonucleotides used for CTA mutagenesis included: the S61Y mutation forward primer, 5′-GGCACGATGATGGATA**C**GT**A**T**A**-CACCTCAATTAGTTTG-3′, and reverse primer, 5′-CAAACTAATTGAGGTG**TA**T**G**TATCCATCATCGTGCC-3′; the V60Y mutagenesis oligonucleotide, 5′-AATTGAGGTAGA**GTA**ATATCCATCATC-3′; and the V60L mutagenesis oligonucleotide, 5′-ACTAATTGAGGTCGA**C**A**G**ATATCCATCATC-3′. (Mutated bases are in bold, and restriction sites included to facilitate screening are underlined.) Oligonucleotides used for DTA mutagenesis included: the Y54S mutation, 5′-GTATTTATTGTCAGTACT**AGA**AAACCCTTTCC-3′; the Y54V mutation, 5′-GTATTTATTGTCAGTACT**AAC**AAACCCTTTCCAATC-3′; and the Y54F mutation, 5′-GTATTTATTGTCAGTACT**AAA**AAACCCTTTCC-3′. The oligonucleotide pair used for the ExoS L342V mutation included the forward primer 5′-CCACGACGACGGCTA**C**G**T**ATCCACCTCCCTGAACC-3′ and the reverse primer 5′-GGTTCAGGGAGGTGGA**TA**C**G**TAGCCGTCGTCGTGG-3′. Antibiotic-resistant clones carrying putative mutations were screened by restriction-digest analysis, where possible, and subsequently sequenced.

Purification of Recombinant CTA1, DTA, ExoS, and Their Respective Mutant Proteins. *Nde*I−*Eco*RI fragments encoding CTA1, DTA, and their respective mutants were cloned from pALTER-*Ex*2 into the expression vector pET-15b (Novagen, Madison, WI), or in the case of CTA1 S61Y and ExoS L342V mutants, mutagenesis was performed in the respective genes cloned into pET-15b. The resulting plasmids were transformed into *E. coli* strain BL21 (DE3) for inducible expression of histidine-tagged proteins from the T7 promoter. The expression of proteins was induced in 1-L cultures with 1.0 mM isopropyl β-D-thiogalactopyranoside (IPTG) (Sigma, St. Louis, MO). Harvested cells were disrupted by two passages through a French pressure cell at 15 000 psi, then centrifuged at 27000*g* at 4 °C for 15 min. Cleared lysates were applied to a nickel-affinity resin according to the manufacturer's specifications, and CTA1 and DTA were eluted with 0.8 M imidazole, while ExoS was eluted with 0.25 M imidazole, as previously described (*7*). Eluate fractions were analyzed by polyacrylamide SDS gel electrophoresis (SDS−PAGE) (*8*), and fractions containing the protein of interest were pooled. CTA1 products were dialyzed against 50 mM potassium phosphate (pH 7.5), 20 mM

dithiothreitol (DTT), 2 mM EDTA, and 10% glycerol. DTA products were dialyzed against 50 mM Tris (pH 8), 1 mM EDTA, and 10 mM DTT. ExoS products were diluted in 25 mM Tris (pH 7.5), 0.05% ovalbumin, and 10% glycerol. Purified (dialyzed) proteins were reduced and denatured in 4X Laemmli sample buffer (*8*) and examined by SDS−PAGE on a 4.5% stacking and 15% resolving gel. The concentration of purified proteins was determined by densitometric analysis of the band corresponding to intact CTA, DTA, or ExoS in Coomassie blue stained gels, using a Color One Scanner and NIH Image Version 1.60. Serially diluted CTA, DTA, or soybean-trypsin inhibitor was used as a standard in densitometry analyses.

ADP-Ribosylation Assay. The DTA ADP-ribosylation of elongation factor 2 (EF-2) was assayed as previously described (*10*), with each 50- or 100-μL reaction mixture containing 50 mM Tris (pH 8.1), 1 mM EDTA, 40 mM DTT, 0.1 μg/mL BSA, 1 μM [*adenine*-^{14}C]NAD, 7.5 μL of partially purified EF-2 (*10*), and the indicated amount of DTA or mutant product. Reactions were incubated for 30 min at 25 °C. ADPRT activity was determined by the incorporation of radiolabeled ADP-ribose into the TCA-precipitable EF-2 fraction and was detected by scintillation counting. ADPRT activity is reported as fmol of product formed.

For the DTA and Y54F kinetic analyses, initial rate data for the ADPRT reaction were determined with respect to NAD binding by varying [*adenine*-^{14}C]NAD concentrations from 0.1 to 4.0 μM at a fixed concentration of EF-2. A nonlimiting concentration of partially purified EF-2 was used in these analyses (*10*), which allowed the determination of a relative K_m for NAD, with each 100-μL reaction containing 22 nM of DTA or Y54F and being allowed to proceed for 15 min at 25 °C. Initial rate data were determined in a similar manner with respect to EF-2's binding by varying concentrations of purified EF-2 from 0.2 to 2.0 μM at a fixed concentration of NAD (6 μM). EF-2 used in these latter reactions was purified as described by Beattie et al. (*11*) and quantified by densitometric analysis as described above using transferrin as a standard. Each 50-μL reaction contained either 10 or 20 nM DTA or Y54F and was allowed to proceed for 16 min at 25 °C. The kinetic parameters were obtained by analysis of Eadie−Hofstee plots from assays performed in duplicate in at least three independent experiments.

CTA1 ADPRT activity was determined using agmatine as the ADP-ribose acceptor, as described by Price et al. (*9*). Each 50-μL reaction mixture contained 50 mM potassium phosphate (pH 7.5); 20 mM DTT; 4 mM $MgCl_2$; 0.1 mM GTP; 2 mM [*adenine*-^{14}C]NAD; 10 mM agmatine; 0.1 mg/mL BSA, with or without 3 μL of a bacterial lysate containing yeastARF1 (described below); and the indicated amount of CTA1 product. Reactions were incubated for 1 h at 25 °C. ADP-ribosylated agmatine was separated from [*adenine*-^{14}C]NAD using an AG1-X2 resin (Bio-Rad Laboratories, Hercules, CA). Radiolabel incorporation into agmatine was detected by scintillation counting and reported as fmol of product formed/min.

A lysate from bacterial cells expressing the cloned yeast ADP-ribosylating factor *ARF1* gene served as the source of ARF in the ADPRT assays. This was prepared by cloning an *Eco*RI cassette containing the *Saccharomyces cerevisiae* *ARF1* gene (kindly provided by Dr. Joseph Dolan, Department of Microbiology and Immunology, Medical University of South Carolina) into the IPTG inducible expression vector pBtac2 (Bio-Rad). After transformation of pBtac2-*ARF1* into *E. coli* strain JM109, *ARF1* expression was confirmed in bacterial lysates by gel electrophoresis, and the indicated amount of lysate was added to assay mixtures.

ExoS ADPRT activity was measured as the incorporation of radiolabeled ADP-ribose into the artificial substrate soybean-trypsin inhibitor, as previously described (*12, 13*). Activity is reported as pmol/min of product formed/μg of purified ExoS.

NAD-Glycohydrolase Assay. DTA NAD-GH assays were performed using a modification of the procedure described by Carroll and Collier (*10*). Each 50- or 100-μL reaction contained 50 mM Tris-HCl (pH 7.8), 0.1 mg/mL BSA, 10 mM DTT, 50 mM NaCl, 36 μM [*carbonyl*-^{14}C]NAD, and the indicated amount of DTA product. Reactions were allowed to proceed for the indicated time and hydrolyzed [^{14}C]nicotinamide was separated from [*carbonyl*-^{14}C]NAD using ethyl acetate extraction (*10*). Radiolabel was quantified by scintillation counting, and the results are reported as pmol of NAD hydrolyzed.

For DTA and Y54F NAD-GH kinetic analyses, initial rate data were collected under conditions where [*carbonyl*-^{14}C]-NAD concentrations were varied from 9 to 36 μM. Each 100-μL reaction contained either 1.2 μM DTA or 1.2 or 2.9 μM Y54F. Reactions were allowed to proceed for 6 h at 25 °C. The kinetic parameters were obtained by analysis of Eadie−Hofstee plots from assays performed in duplicate in at least three separate experiments.

CTA1 NAD-GH assays were performed using a modification of the procedure described by Moss et al. (*14*) Each 50-μL reaction contained 50 mM potassium phosphate (pH 7.5), 20 mM DTT, 4 mM $MgCl_2$, 145 μM [*carbonyl*-^{14}C]-NAD, and the indicated amount of CTA1 product. Although ARF is known to enhance CT NAD-GH activity (*15*), all assays were performed in the absence of ARF, because the bacterial lysate form of ARF used in these studies was found to interfere with the NAD-GH assay. Samples were incubated for 4 h at 25 °C. Hydrolyzed [^{14}C]nicotinamide was separated, quantified as described in the DTA NAD-GH assay, and reported as fmol of NAD hydrolyzed.

Proteolysis. Limited trypsinolysis of DTA or the DTA mutant proteins was performed by incubating 2 μg of purified protein with sequencing-grade modified trypsin (Promega V5111) at a 1/4000 (wt/wt) trypsin/DTA protein ratio at 25 °C in a total volume of 40 μL of 20 mM Tris-HCl (pH 7.5), 20 mM DTT, for the indicated times. Limited trypsinolysis of CTA1 or CTA1 mutant proteins was performed by incubating 0.75 μg of purified protein with trypsin type XIII (Sigma T8642) at a 1/30 (wt/wt) trypsin/CTA1 protein ratio at 25 °C for the indicated times in a total volume of 30 μL of 50 mM potassium phosphate (pH 7.5). CTA1 trypsinolysis studies were also performed using sequencing-grade modified trypsin at a 1/800 (weight/weight) trypsin/CTA1 product ratio, and similar results were obtained. Proteolysis reactions were terminated by the addition of 4X Laemmli sample buffer containing β-mercaptoethanol (*8*) and by heating at 95 °C for 3 min. Products were resolved by SDS−PAGE on a 4.5% stacking gel and 15% resolving gels (*8*) and were detected by Coomassie blue staining for the DTA or by

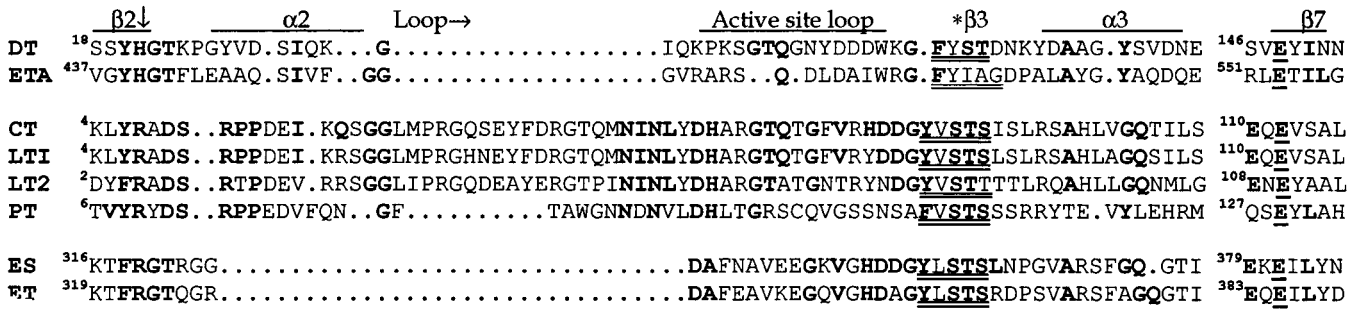

FIGURE 1: Alignment of residues that form the NAD binding cleft within the common core-fold of ADP-ribosylating toxins. The structural alignment of core regions of ETA, CT, LT1, LT2, and pertussis toxin (PT) with DT used the Cα atoms and the algorithm of Kabsch (*36*), as previously described (*2*). ExoS (ES) and ExoT (ET) were aligned on the basis of sequence homology and molecular modeling studies, as previously described (*5, 37*). Residues forming structurally equivalent motifs based on this alignment are located under the line, and the motifs are labeled relative to the DT structure. The conserved β3-strand sequence is double underlined, and the asterisk identifies the residue within DT, CT, and ExoS β3-strand which was the focus of these studies, with the down arrow locating the predicted functional counterpart of these β3-strand residues in their respective β2-strands. The catalytic glutamic acid residue in the discontiguous β7-strand is underlined. Bold print highlights sequence homology recognized among different toxins, dots mark spacing introduced for sequence alignment, and superscript numbers identify the position of specific residues in the protein.

immunoblot analysis (*16*). The immunoblot analysis used a rat polyclonal antiserum prepared against purified CTA as previously described (*17*) and peroxidase-conjugated goat anti-rat IgG (Sigma).

Fluorescence Quenching. A decrease in DTA intrinsic fluorescence quenching as a function of increasing NAD concentration was measured as previously described (*18*). Solutions of purified DTA, Y54S, Y54V, and Y54F (0.4 μM) were excited at 285 nm (4-nm band-pass) and the fluorescence intensity was measured at 335 nm (8-nm band-pass) using an SLM Aminco fluorimeter (model 8000). The fluorescence decrease of L-tryptophan (0.4 μM) as a function of NAD concentration was used to correct for NAD self-quenching. Relative fluorescence upon the addition of increasing concentrations of NAD was compared for each protein in analyses performed in parallel, in two independent studies. Identical patterns of quenching were observed in the two studies, and mean relative fluorescence obtained for the individual proteins in these two studies is reported.

Photoaffinity Labeling. The binding of NAD to the DTA and mutant DTA proteins was examined in photoaffinity-labeling studies by monitoring the incorporation of radioactivity from [*carbonyl*-^{14}C]NAD into TCA-precipitable DTA product, as previously described (*19*), with the following modifications: Reaction mixtures contained a fixed amount of DTA or mutant DTA (3−5 μM), and increasing concentrations of NAD (2.5−40 μM) were added to a total volume of 25 μL in 50 mM Tris (pH 7.5). Cross-linking reactions were performed on ice by irradiating samples at 254 nm for 30 min using a Mineralight (model UVG11-15, UVP, Inc.) positioned at a fixed distance of 5.5 cm from the samples. The specificity of [*carbonyl*-^{14}C]NAD binding to the DTA was confirmed using unlabeled NAD, with 40 μM unlabeled NAD inhibiting the binding of 20 μM [^{14}C]NAD by 92%. The relative cross-linking of the DTA and DTA mutants to NAD was compared in reactions performed in parallel in two independent studies. The relative cross-linking efficiency of the individual proteins was similar in both studies, and results from one study are reported.

RESULTS

Design and Production of NAD Binding Cleft Mutant ADPRT Toxins. Although the active-site regions of ADPRT toxins include a common core structure, only limited sequence homology is apparent when residues within this region are aligned based on their Cα atom structure (*1, 2*) (Figure 1). To examine how the sequence diversity within the NAD binding cleft relates to function, we genetically exchanged residues in the most highly conserved region of the active-site cleft of ADPRT toxins, the β3-strand, which is aligned in Figure 1 and predicted to be functionally equivalent. Mutations were performed in the cloned genes encoding the enzymatically active portions of DT, residues 1−193 (DTA), or CT, residues 1−192 (CTA1). Analysis of induced products found DTA to fractionate to the supernatant of the bacterial lysate, while a large portion of CTA1 fractionated to the pellet. To obtain sufficient concentrations of products in their natural, soluble form for functional analyses, DTA, CTA1, and their respective mutants were cloned into pET-15b, which, via the added amino-terminal histidine tag, allowed the enrichment and purification of the individual proteins.

Exchange of Tyr54 in the β3-Strand of DTA for a Serine Residue. NAD-cocrystallization studies implicate a direct role of Tyr54 in the β3-strand of DT in NAD binding, and the absence of an analogous tyrosine residue in the CT group has been predicted to differentiate the binding of DT to NAD from that of CT (*5*). To directly compare the mechanisms of NAD binding by DT and CT, Tyr54 in DTA was mutated to its functional homologue in CT, Ser61 (Y54S mutant). A Tyr54-to-valine mutation was performed in conjunction with these studies (Y54V mutant), Val60 being adjacent to S61 in the CT NAD binding cleft. Analyses of purified products from the DTA and the Y54S and Y54V mutant clones identified proteins of identical electrophoretic mobility on SDS−PAGE (Figure 2A). When assessed for structural alterations based on limited trypsinolysis, both the mutant and wild-type DTA produced two predominant proteolytic fragments of identical mass, although, on the basis of relative band intensities, the DTA appeared more resistant to proteolysis than the Y54S or Y54V mutant (Figure 2B). These analyses indicate that, while accessibility to the wild-type DTA tryptic cleavage sites might be slightly altered in the Y54S and Y54V mutants, the mutations do not cause global alterations in structure that allow accessibility to new cleavage sites.

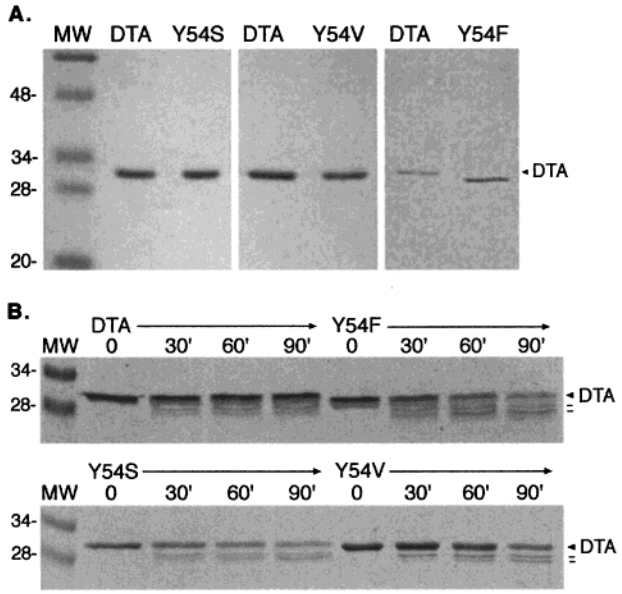

FIGURE 2: Analyses of DTA and DTA β3-strand mutant proteins. A. Comparison of purified DTA, Y54S, Y54V, and Y54F proteins. Histidine-tagged proteins were induced by IPTG in cultures of *E. coli* BL21 (DE3) containing the indicated pET15b-DTA construct. Cleared bacterial lysates were applied to a Ni-affinity resin, washed, then eluted with 0.8 M imidazole. Fractions containing the indicated proteins were pooled, dialyzed, denatured, and reduced in Laemmli sample buffer (*8*), resolved by SDS−15% PAGE, and stained with Coomassie blue. The slightly faster electrophoretic mobility of the Y54F mutant has been detected in multiple independently produced and purified Y54F preparations. B. Trypsinolysis of DTA and DTA mutant proteins. The indicated purified DTA proteins (2 μg) were digested with trypsin at a 1/4000 (wt/wt) trypsin/DTA protein ratio for 0, 30, 60, or 90 min at 25 °C. Reactions were terminated by the addition of 4X Laemmli sample buffer containing β-mercaptoethanol and heating at 95 °C for 3 min. Peptides were resolved by SDS−PAGE and stained with Coomassie blue. Prestained molecular mass markers (MW) and the DTA are labeled, and the two predominant proteolytic fragments are marked.

When the ADPRT activity of DTA, Y54S, and Y54V was compared, the specific activity of the DTA was 10 309 fmol μg^{-1} min^{-1}, while that of the Y54S and Y54V mutants was 48 and 21 fmol μg^{-1} min^{-1}, respectively (Figure 3A; the inset graph shows the slightly higher activity of the Y54S mutant). The approximate 200- or 500-fold decrease in activity of the two mutants correlated with severely reduced NAD-GH activity, which decreased from that of DTA (172 fmol μg^{-1} min^{-1}) to levels less than or equal to that of control reactions containing no enzyme (Figure 3B). The significant decrease in enzymatic activity resulting from the Y54S and Y54V mutations, in association with limited structural alterations, supports the importance of Tyr54 to the function of the DTA NAD binding cleft.

Mutation of Tyr54 in DTA to a Phenylalanine Residue. To examine the functional role of an aromatic moiety at position 54 in the DTA active-site cleft, and to explore the possible role of the hydroxyl group on Tyr54 in the ADPRT reaction, Tyr54 was mutated to a phenylalanine (Y54F mutant). Comparisons of purified DTA and Y54F found the Y54F mutant to have a slightly faster mobility than the DTA when resolved by SDS−PAGE (Figure 2A), which was a reproducible characteristic of the Y54F mutant upon multiple rounds of purification. Limited trypsinolysis of the Y54F mutant identified two predominant proteolytic fragments,

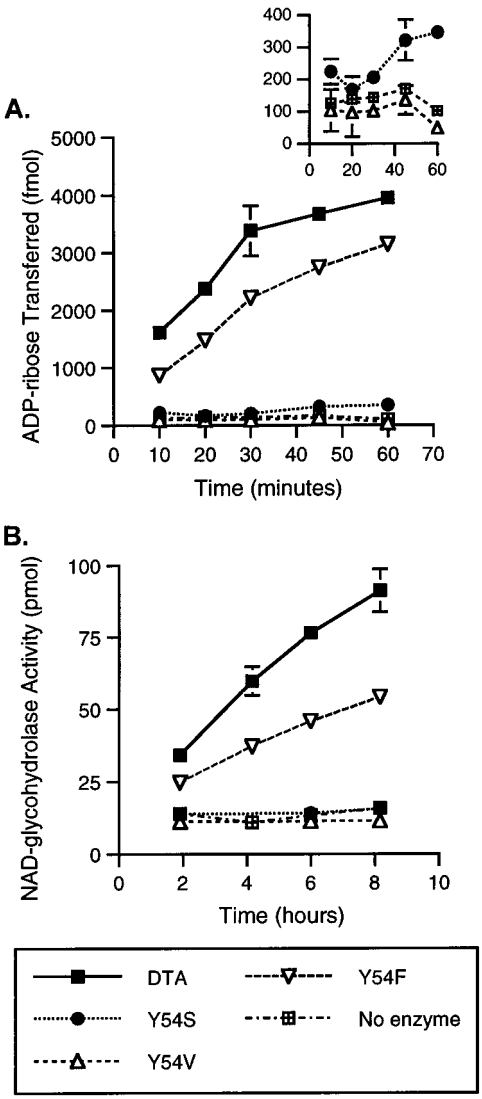

FIGURE 3: Enzymatic activity of DTA and Y54S, Y54V, or Y54F DTA mutant proteins. A. ADPRT activity. Purified DTA (0.01 μM), Y54S (0.2 μM), Y54V (0.2 μM), and Y54F (0.01 μM) were assayed for their ability to transfer radiolabeled ADP-ribose from [*adenine*-^{14}C]NAD to the TCA-precipitable EF-2 fraction. Each 50-μL reaction contained 7.5 μL of partially purified EF-2, 1 μM [*adenine*-^{14}C]NAD, and the indicated purified protein or no enzyme and was allowed to proceed at 25 °C for the time indicated. Results are expressed as fmol of ADP-ribose transferred. Each point represents the mean and standard deviation (SD) of samples assayed in triplicate. One representative assay of at least three independent analyses is shown. The inset graph shows the slightly greater ADPRT activity of the Y54S mutant on an expanded scale. B. Glycohydrolase activity. NAD-GH activity was determined by incubating the purified DTA (1.2 μM), Y54S (1.5 μM), Y54V (1.6 μM), Y54F (1.5 μM), or no enzyme with 36 μM [*carbonyl*-^{14}C]-NAD at 25 °C for the indicated time. Released [^{14}C]nicotinamide was separated from the [*carbonyl*-^{14}C]NAD by ethyl acetate extraction. Results are expressed as pmol of NAD hydrolyzed. The mean and SD of samples assayed in triplicate from one representative assay of at least three independent analyses are shown.

similar to that of DTA, but shifted in relative mass in association with the faster mobility of the Y54F mutant (Figure 2B). The Y54F mutant also appeared to be digested at a slightly faster rate than that of DTA, indicating an increase in accessibility to normal DTA tryptic cleavage sites. Thus, like the Y54S and Y54V mutants, the lack of accessibility of new tryptic cleavage sites in the Y54F mutant supported that minimal structural alterations occurred upon

Table 1: Relative Kinetic Parameters of DTA and Y54F Proteins[a]

A. NAD-GH

	DTA	Y54F
K_m(NAD) (μM)	9.59 ± 5.63	15.84 ± 5.19
V_{max} (fmol μg^{-1} min^{-1})	290 ± 70	55 ± 16
k_{cat}/K_m (M^{-1} min^{-1})	645	72.9

B. ADPRT

	DTA	Y54F
(i) Fixed (EF-2), Variable (NAD)		
K_m(NAD) (μM)	1.55 ± 0.21	1.92 ± 0.41
V_{max} (pmol μg^{-1} min^{-1})	102.11 ± 4.94	70.45 ± 20.17
k_{cat}/K_m (M^{-1} min^{-1})	1.38 × 10^6	0.70 × 10^6
(ii) Fixed (NAD), Variable (EF-2)		
K_m(EF-2) (μM)	0.59 ± 0.32	0.58 ± 0.22
V_{max} (pmol μg^{-1} min^{-1})	108.26 ± 2.71	80.90 ± 0.14
k_{cat}/K_m (M^{-1} min^{-1})	3.85 × 10^6	2.93 × 10^6

[a] Kinetic parameters were obtained by analyses of Eadie−Hofstee plots.

removal of a hydroxyl moiety from Tyr54, even though an alteration in SDS−PAGE mobility was detected.

Unlike the Y54S and Y54V mutants, however, the Y54F mutant was found to retain high levels of enzymatic activity. In ADPRT assays, the Y54F mutant had a specific activity of 6635 fmol μg^{-1} min^{-1}, which was 64% of that of DTA (Figure 3A). The NAD-GH activity of the Y54F mutant was correspondingly 52% of that of DTA (Figure 3B). The specific activity of DTA is 185 fmol μg^{-1} min^{-1}, compared to 96 fmol μg^{-1} min^{-1} for Y54F. The 1.6-fold reduction in the ADPRT activity of the Y54F mutant, as compared to the 200- or 500-fold reduction in activity of the Y54S or Y54V mutants, respectively, supports the involvement of an aromatic moiety at position 54 in the enzymatic reaction of DTA. The 40−50% reduction in enzymatic activity following the Y54F mutation, however, also identifies the role of the phenolic hydroxyl group of Tyr54 for maximal DTA enzymatic function.

Kinetic Analyses of the DTA Y54F Mutant. Kinetic analyses were performed on the Y54F mutant to further understand the role of Tyr54 in the DT enzymatic reaction. For the NAD-GH reaction, initial rate data were collected for DTA and Y54F, with NAD concentrations varying from 0.9 K_m to 3.7 K_m. Relative kinetic parameters, obtained from Eadie−Hofstee plots, are summarized in Table 1A. A slight, but not statistically significant, increase was observed in the relative K_m for NAD of Y54F in the NAD-GH reaction, with the K_m of DTA and Y54F calculated to be 9.59 and 15.84 μM, respectively. This corresponds closely to the previously reported K_m for NAD of DTA of 11.0 μM (*18*). In comparison, the relative V_{max} of Y54F was calculated to be approximately 5-fold less than that of DTA, 290 fmol μg^{-1} min^{-1} versus 55 fmol μg^{-1} min^{-1}, suggesting that the Y54F mutation has a greater effect on NAD hydrolysis than NAD binding. Effects on both K_m and k_{cat} contribute to the decreased activity of the Y54F mutant, though, as indicated by the 9-fold decrease in the second-order rate constant, k_{cat}/K_m, of Y54F when compared to that DTA.

The kinetic parameters of the DTA and Y54F were further compared in the DTA ADPRT reaction (Table 1B). The K_m for the NAD of the DTA and the Y54F was determined from initial rate data with the NAD concentrations varying from 0.06 to 2.6 times that of the calculated K_m. The use of a nonlimiting concentration of partially purified EF-2 allowed the calculation of a relative K_m for the NAD of the Y54F of 1.92 μM, which was slightly, but not significantly, higher than that of the DTA of 1.55 μM. A 1.5-fold decrease in the relative V_{max} of the Y54F was also detected, with the relative V_{max} of the Y54F calculated to be 70 pmol μg^{-1} min^{-1} versus that of DTA, 102 pmol μg^{-1} min^{-1}. The relative K_m for the EF-2 of the DTA and the Y54F in the ADPRT assay was determined from initial rate data using 20 and 10 nM concentrations of each enzyme, a fixed concentration of NAD (6 μM), and concentrations of chromatographically purified EF-2 varying from 0.2 K_m to 2 K_m. In these analyses, no difference was observed in the K_m for the EF-2 of the DTA and the Y54F (0.59 and 0.58 μM, respectively), with a 1.3-fold reduction in the V_{max} of the Y54F mutant. Together the kinetic analyses of the NAD-GH and ADPRT reactions indicate that the Y54F mutation had a greater effect on the catalytic activity of DTA, with lesser effects on NAD binding. The Y54F mutation appeared to have no effect on EF-2 binding.

Analysis of NAD Binding by Tyr54 DTA Mutant Proteins. To directly examine the ability of alternative residues at position 54 in DTA to function in NAD binding, the intrinsic fluorescence of DTA relative to increasing NAD concentrations was compared with that of the DTA Y54 mutant proteins. Analyses using a fixed 0.4 μM concentration of purified proteins with increasing concentrations of NAD, ranging from 0 to 400 μM, revealed similar fluorescence quenching of the DTA and the Y54F and Y54S mutants (Figure 4A). In comparison, the Y54V mutant showed no loss of intrinsic fluorescence relative to increasing NAD concentrations, indicating a loss of NAD binding. Photoaffinity cross-linking studies were performed as an alternative method of assessing the association of NAD within the active-site cleft. In these studies, NAD was found to be cross-linked to the Y54F mutant approximately 75% as efficiently as to DTA, while the cross-linking efficiency to the Y54S mutant was 50% of that to the DTA (Figure 4B). The Y54V mutant showed the least efficient cross-linking with NAD. One explanation for the apparent differences observed in the association of NAD with the Y54F and Y54S mutants in fluorescence quenching and cross-linking studies is that the latter method was able to detect an altered positioning of NAD within the respective active-site clefts. In the Y54F mutant, this repositioning may be reflected in its reduced enzymatic activity. In the Y54S mutant, which lacks an aromatic moiety, NAD cross-linking efficiency does not correlate with enzymatic activity. Both fluorescence quenching and NAD cross-linking studies, however, support the ability of a serine to substitute for Tyr54 in forming a functional NAD binding cleft. This contrasts with enzymatic assays which found a serine unable to substitute for an aromatic residue in the hydrolysis of NAD.

Functional Comparison of the CTA1 β3-Strand to the β3-Strand of DTA. Reciprocal mutagenesis studies were performed in CTA1 to evaluate the functional relationship of residues within the β3-strand of the NAD binding cleft of CTA1 and functional homologues within the NAD binding cleft of DTA. Ser61 of CT is the predicted functional homologue of Tyr54 in DT, contributing both to NAD binding and active-site cleft integrity. Initially, to examine

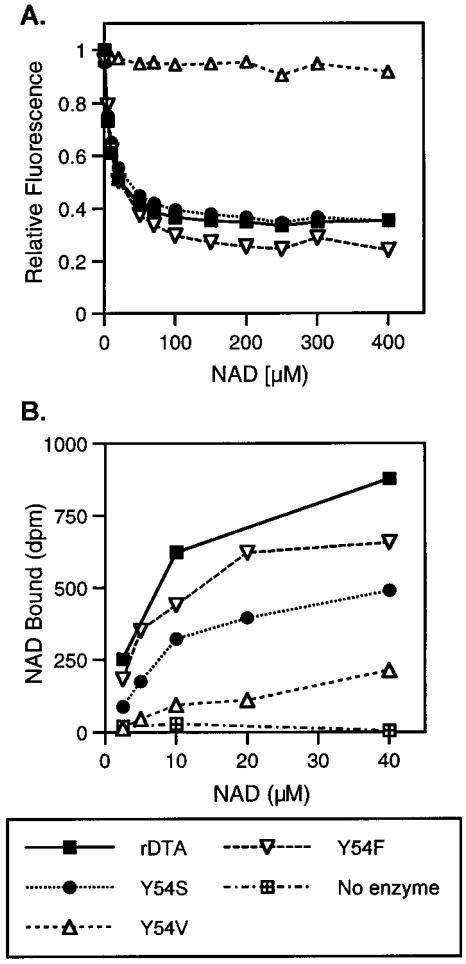

FIGURE 4: Analysis of NAD binding to DTA and Y54S, Y54V, or Y54F DTA mutant proteins. A. NAD fluorescence quenching. The binding of NAD to the DTA and the DTA mutant proteins was determined by monitoring the decrease in intrinsic fluorescence quenching as a function of increasing NAD concentration. Analyses were performed using the indicated purified proteins (0.4 μM) and concentrations of NAD ranging from 0 to 400 μM. Solutions were excited at 285 nm (4-nm band-pass), and the fluorescence intensity was measured at 335 nm (8-nm band-pass). Data were corrected for NAD self-quenching, and the percent quenching at each NAD concentration is shown. The mean fluorescence quenching detected in two independent analyses is shown. B. NAD-photoaffinity cross-linking. The association and positioning of NAD within the DTA and the mutant DTA proteins was determined in photoaffinity-labeling studies by monitoring the incorporation of radioactivity from [*carbonyl*-^{14}C]NAD into TCA-precipitable protein. Cross-linking was performed by irradiating 3−5 μM DTA product and increasing concentrations of NAD at 254 nm for 30 min at 0 °C. Representative results from one of two independent assays are shown.

whether a tyrosine residue could function in NAD binding in the CT active-site cleft, a direct Ser61 to tyrosine mutation was performed in CTA1 (S61Y mutant). An alternative mutational strategy, Val60-to-tyrosine mutation, was also used to introduce a tyrosine in the NAD binding cleft of the CTA1. A second strategy was attempted because previous studies by Harford et al. (*20*), found that an S61F mutation in the highly homologous LT, produced a nontoxic protein, making it unlikely that a similar S61Y mutation in CTA1 would produce a functional protein. Substituting Val60 in CTA1 with a tyrosine (V60Y mutant) positioned the tyrosine adjacent to the functionally conserved Ser-Thr-Ser amino acid triad in the CT group β3-strand sequences. This

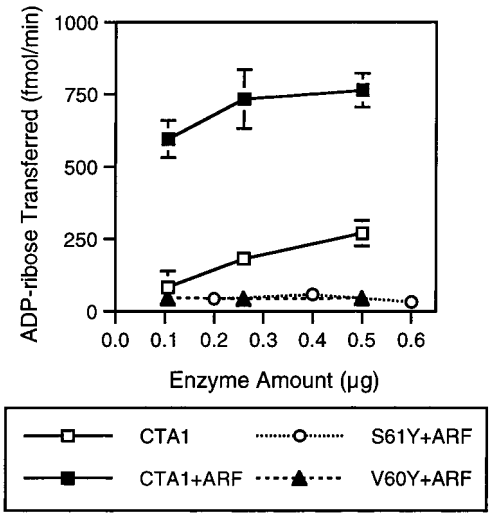

FIGURE 5: Enzymatic activity of CTA1 and S61Y or V60Y mutant proteins. Increasing amounts of purified CTA1, S61Y, or V60Y were assayed for their ability to transfer radiolabeled ADP-ribose from [*adenine*-^{14}C]NAD to the artificial substrate agmatine. Each 50-μL reaction contained 10 mM agmatine, 2 μM [adenine-^{14}C]-NAD, and the indicated amount of protein and was allowed to proceed for 1 h at 25° C in the presence or absence of 3 μL of an ARF-containing cell lysate. ADP-ribosylated agmatine was separated from [*adenine*-^{14}C]NAD using an AG1-X2 resin. Results are expressed as fmol of ADP-ribose transferred/min, and each point represents the mean and standard error (SE) of samples assayed in duplicate in two independent assays.

produced a β3-strand sequence of YYSTS, which closely resembled the functional FYST β3-strand sequence of DT. When assayed for ADPRT activity in the presence of ARF, activities of the V60Y and S61Y mutants remained at baseline levels, ~100 fmol μg^{-1} min^{-1}, which compared to that of the CTA1 at 3216 fmol μg^{-1} min^{-1} (Figure 5). As would be predicted on the the basis of the location of these mutations within the NAD binding cleft, the loss in ADPRT activity of the V60Y and S61Y mutants reflected a loss in NAD-GH activity. The NAD-GH activity of both mutants was below baseline levels (<140 fmol μg^{-1} min^{-1}), while that of the CTA1 was 2588 ± 303 fmol μg^{-1} min^{-1}.

Analyses of purified V60Y and S61Y proteins identified products of the same mobility as that of the CTA1; however, both higher- and lower-molecular mass products were evident in the lanes of the mutant proteins, indicating their altered stability (Figure 6A). Analyses of structural alterations based on limited trypsinolysis found the CTA1 to be somewhat resistant to trypsin, with digestion requiring a 2-h exposure to trypsin. No proteolytic products were detected at intermediate time points (Figure 6B,C). Structural alterations in V60Y and S61Y were recognized by increased, rather than decreased, resistance to trypsinolysis and the production tryptic peptides which differed from that of wild-type CTA1. The increased resistance of the CTA1 β3-strand mutants to trypsinolysis, when compared to CTA1, was similar to results previously reported for the S63K β3-strand LT mutant when compared to wild-type LT (*21*). It is notable that while the S61Y and V60Y mutants appeared to be more sensitive to degradation during purification procedures, they remained more resistant to specific tryptic cleavage. The alteration of proteolytic-cleavage products observed following the introduction of a tyrosine residue into the β3-strand of the CTA1 is consistent with these mutations causing more global

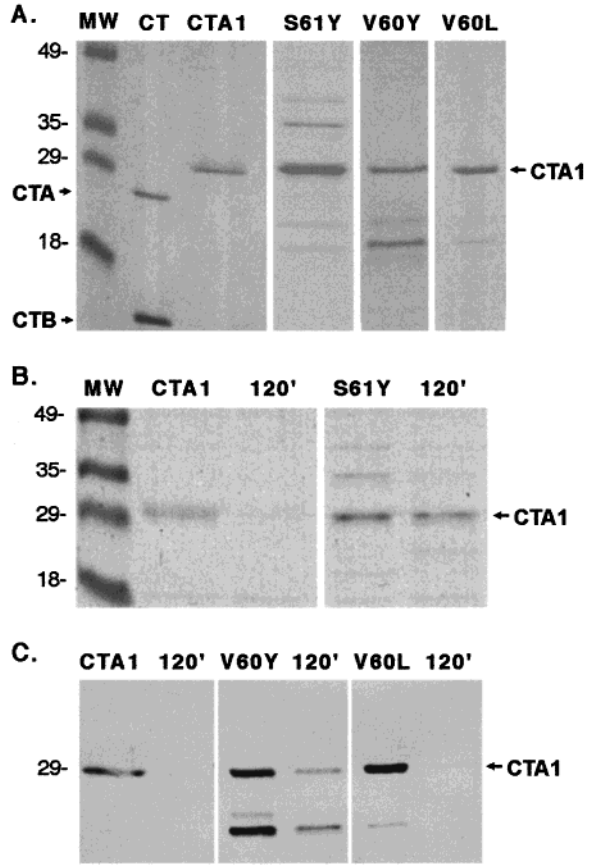

FIGURE 6: Analyses of CTA1 β3-strand mutant proteins. A. Comparison of purified CTA1, S61Y, V60Y, and V60L proteins: Histidine-tagged proteins were produced, Ni-affinity purified, and processed as described in Figure 2A; resolved by SDS−PAGE; and stained with Coomassie blue. S61Y and V60Y lanes show higher molecular mass aggregates and/or putative proteolytic products, which are less evident in the V60L lane. Trypsinolysis of CTA1 and CTA1 mutant proteins: The indicated purified proteins (0.75 μg) were digested with trypsin at a 1/30 (wt/wt) trypsin/CTA1 protein ratio for 0, 30, 60, or 120 min at 25 °C. The most notable alterations in trypsinolysis patterns, which occurred at 120 min, are shown. Reactions were terminated by the addition of 4X Laemmli sample buffer containing β-mercaptoethanol and heating at 95 °C for 3 min. Peptides were resolved by SDS-15% PAGE and either stained with Coomassie blue (B) or transferred to nitrocellulose and detected with a rat-CTA-specific antiserum and a peroxidase-conjugated goat anti-rat immunoglobulin (C). The S61Y mutation caused a decrease in recognition by the CTA antiserum, preventing immunoblot assessment. Prestained molecular mass markers (MW) are labeled in **A** and **B** and referenced in **C**. CTA, CTB, and CTA1 are labeled. The higher molecular mass of CTA1 than CTA reflects the addition of residues from the pET-15b vector, including the histidine tag.

structural alterations, which preclude interpretations of their direct effects on function. Both the loss of function and structure of these mutants, however, are consistent with CTA1 being unable to utilize tyrosine in a similar manner as does DT in its mechanism of NAD hydrolysis.

Examination of CTA1 NAD Binding Cleft Structure Relative to Function. To gain further insight into the relationship between the CTA1 NAD binding cleft structure and its function, the effect of a more conservative CTA1 β3-strand mutation on function was examined. ExoS is functionally similar to CT in that both toxins: (1) transfer an ADP-ribose moiety to arginine residues in their target proteins (*22*, *23*), (2) have less discriminate protein substrate specificity in vitro (*23*−*26*), and (3) require eukaryotic cofactors for maximal activity, the cofactor ARF enhancing CT enzymatic activity (*27*), while ExoS requires 14-3-3 proteins for maximal ADPRT activity (*28*). Consistent with their functional similarities, CT and ExoS have a high degree of sequence homology in the region surrounding the β3-strand sequence and differ by only one residue within the β3-strand (Figure 1). CT has a valine residue in the second position (Val60), while ExoS has a leucine residue at an equivalent position (Leu342). The functional similarities between these two toxins, along with the similar properties of the valine and leucine residues, favor that a Val60-to-leucine mutation in CTA1 would have minimal effects on both structure and function.

Analysis of the purified Val60-to-leucine CTA1 (V60L) mutant by SDS−PAGE and limited trypsinolysis revealed products and digestion patterns closely resembling that of the CTA1 (Figure 6), indicating that structural alterations in the V60L mutant were more limited than those observed for the V60Y or S61Y mutants. However, V60L mutant ADPRT activity was found to remain at baseline levels like the other CTA1 β3-strand mutants, the V60L mutant having an activity of ~43 fmol μg^{-1} min^{-1} when assayed in the presence of ARF, which compared to that of the CTA1 at 2173 ± 915 fmol μg^{-1} min^{-1}. Again the decreased ADPRT activity of the V60L mutant directly reflected a loss of NAD-GH activity, with the NAD-GH activity of the CTA1 being 2588 ± 303 and that of the V60L mutant less than baseline levels. The loss of enzymatic activity following the conservative exchange of a valine for a leucine residue, combined with evidence of limited structural alteration, implies either the direct role of Val60 in CTA1 function or that the function of the CTA1 is highly dependent on the positioning of the Val60 residue within the NAD binding cleft.

While low levels of enzymatic activity of the V60L mutant, as well as the high K_m of CT for NAD (~4 mM) (*29*), precluded kinetic or NAD binding studies of the V60L mutant, further understanding of the structural versus functional roles of Val60 in the ADPRT reaction was indirectly obtained through reciprocal mutagenesis studies performed in the cloned ExoS structural gene. When Leu342 in ExoS was mutated to a valine (L342V mutant), making the predicted β3-strand sequence of ExoS identical to that of CT, no loss of ADPRT activity was detected, with the ExoS and the L342V mutant activities being 29.3 and 39.0 pmol μg^{-1} min^{-1}, respectively. The finding that a valine can function in place of, and possibly slightly better than, a leucine at this site in ExoS supports that these residues have the potential to be functionally interchangeable. The loss of activity of the V60L CTA1 mutant, while the reciprocal L342V ExoS mutant retains function, supports that it is the repositioning caused by introduction of a leucine residue into the β3-strand of CTA1 that disrupts the NAD binding cleft function. This draws attention to the restricted sequence and/or structural flexibility allowed the CTA1 β3-strand in forming a functional active site.

DISCUSSION

Studies of structure−function relationships of ADP-ribosylating proteins provide a unique opportunity for envisioning how a common enzymatic function can be performed by different mechanisms. Numerous bacterial toxins and endogenous eukaryotic proteins share an ADPRT mechanism of action, and the structural alignment of residues

that form the active site of ADP-ribosylating proteins provides clues as to how ADPRT activity is maintained among proteins that have diverse substrate specificities. Studies described in this paper focused on understanding the functional relationship of residues that form the structurally conserved β3-strand sequence within the NAD binding cleft of ADP-ribosylating toxins. Variations in this sequence have been proposed to differentiate mechanisms of NAD binding by ADP-ribosylating proteins (*5*). The premise of our studies was that insight into differences in the mechanism of NAD binding and hydrolysis by ADP-ribosylating toxins could be gained by examining how residues predicted to be functional homologues in β3-strand sequences function in the context of different ADP-ribosylating toxins.

The structural alignments of the Cα atoms of ADP-ribosylating toxins by Sixma et al. (*1*) and Bell and Eisenberg (*2*) were used in the design of mutations to explore the functional interrelationship of residues predicted to be integral to the NAD binding in β3-strand sequences. Our studies focused on DT and CT, which define the two toxin NAD binding groups. Tyr54 in the β3-strand of DT has been implicated in NAD binding, with the aromatic rings of Tyr54 and Tyr65 facilitating the stacking of the nicotinamide portion of NAD in the DT active-site cleft (*2*). The predicted functional homologue in CT of Tyr54 is Ser61, and the presence of a serine residue rather than a tyrosine in the β3-strand of CT is thought to differentiate its mechanism of NAD binding from that of DT (*5*).

The functional interrelationship of Tyr54 in DT and Ser61 in CT was directly examined in reciprocal mutagenesis studies, first replacing Tyr54 in the DTA for a serine. The Y54S DTA mutant retained NAD binding, but it was unable to hydrolyze NAD. A Y54V mutation in DTA, in comparison, resulted in a loss of both NAD binding and hydrolysis. The ability of a serine to replace the function of Tyr54 in NAD binding in the DTA β3-strand is consistent with the DT active site maintaining a mechanism of NAD binding similar to that of CT.

The efficient binding of the Y54S DTA mutant to NAD, but loss of enzymatic activity, implicated a catalytic role of the aromatic portion of Tyr54 in NAD hydrolysis. This role was supported by a Tyr54-to-phenylalanine mutation, which found the Y54F mutant to retain 64% and 52% of the DTA ADPRT and NAD-GH activity, respectively. In kinetic analyses of the Y54F mutant, the loss of the phenolic hydroxyl group from the tyrosine residue had a greater impact on the catalytic efficiency of the NAD-GH reaction than on NAD binding. The Y54F mutation also appeared to have less effect on the V_{max} and K_m of the ADPRT reaction than of the NAD-GH reaction. This latter difference may be attributable to a stabilizing effect of EF-2 on the enzymatic transition complex, as previously described in DTA Trp50 mutational studies (*30*). Consistent with this possibility, the Y54F mutation did not affect binding to EF-2. Reduction in ADPRT activity by the Y54F mutation contrasts with previous ETA studies which found that substitution of Tyr470 with a phenylalanine (Tyr470 being the ETA analogue of Tyr54 in DT) resulted in no loss of enzymatic activity (*31*). The role of the phenolic hydroxyl group of Tyr54 in DT enzymatic function thus may differentiate the active-site structure of DT from that of ETA.

Structural analyses of Y54F, Y54S, and Y54V, based on limited trypsinolysis, revealed similar peptide fragments in digests of mutants and wild-type DTA, but the mutant proteins appeared to be digested at a slightly greater efficiency. These results are consistent with the Tyr54 mutations causing local alterations in protein structure in association with their effects on NAD binding and hydrolysis, rather than global structural alterations, which would be predicted to expose new tryptic-cleavage sites in the DTA which contains many lysine and arginine residues.

Together, structural and functional comparisons of the Y54F, Y54S, and Y54V DTA mutants support that Tyr54 plays a bifunctional role in the ADPRT reaction. The hydroxyl moiety of tyrosine (or serine) allows the formation of a functional NAD binding cleft, while the aromatic portion of tyrosine (or phenylalanine) is required for catalytic activity. NAD cross-linking studies provide evidence that Tyr54 may function in the positioning NAD within the active-site cleft. The decreased cross-linking efficiency of NAD with the Y54S mutant, and to some extent with the Y54F mutant, when compared to wild-type DTA would be consistent with NAD being positioned differently in the active-site clefts of these mutants. The altered positioning of NAD within the active-site cleft relative to its efficiency of hydrolysis may be reflective of previous studies of Bell et al. (*32*), who found that NAD bound to DT had an altered conformation that was predicted to favor catalysis. It is currently unknown how the faster SDS−PAGE mobility of the Y54F mutant, in association with the loss of a hydroxyl group from Tyr54, might relate to the slight loss of enzymatic activity or the positioning of NAD within the active site of this mutant.

While analyses of the functional relationship of Tyr54 in DT to Ser61 in CT provided an increased understanding of the mechanism of NAD binding and hydrolysis within the DTA active site, reciprocal studies in CTA1 proved more difficult to interpret. Positioning a tyrosine either in place of Ser61 in the CTA1 β3-strand or in place of Val60 (retaining the functionally conserved Ser-Thr-Ser β3-strand triad) resulted in a loss of enzymatic activity. Both mutations, however, were associated with altered tryptic-cleavage patterns, which is indicative of global structural alterations and precludes direct functional comparisons of the serine and tyrosine residues within the CTA1 β3-strand. Although it might be speculated that Tyr59 in the CT β3-strand could function as the homologue of Tyr54 in DT, mutating this residue in LT to a methionine resulted in no loss of toxicity (*33*), indicating its lack of involvement in the enzymatic reaction. In the crystallographic structure of LT, which is highly homologous to CT, Ser61 hydrogen-bonds with Arg7 (*34*) and is predicted to function in the maintenance of the NAD binding cleft. The importance of Ser61 in CT function was first recognized in mutagenesis studies of LT, where the substitution of Ser61 for phenylalanine was found to abrogate LT toxicity (*20*). Subsequent kinetic analyses of a more conservative Ser61-to-threonine mutation in LT found the mutation to have minimal effect on NAD binding and only a 10-fold reduction in catalytic activity (*35*). While all data are consistent with the hydroxyl moiety of serine (or threonine) in CTA1 functioning in a manner similar to that of the hydroxyl group of Tyr54 in DTA in the formation of a functional CTA1 NAD binding cleft, the collective finding

that a tyrosine residue at position 59, 60, or 61 is either not involved in or does not allow CT (or LT) function is consistent with CT having acquired a different mechanism of NAD hydrolysis.

Functional constraints on the CTA1 active-site cleft became further evident when a conservative V60L CTA1 mutation was performed, converting the β3-sequence to that of the closely related toxin, ExoS. Valine and leucine have similar hydrophobic properties, and only minor structural alterations were apparent upon the conservative V60L exchange in the CTA1 β3-strand. Consequently, the loss of enzymatic activity caused by this mutation was not anticipated. Reciprocal studies in ExoS, mutating Leu342 (the predicted functional homologue of Val60 in CT) to a valine, resulted in no loss of function, confirming that the valine and leucine residues have the potential to perform an equivalent function within the ExoS active site. The inability of an apparently functionally equivalent leucine residue to function in place of Val60 in CTA1 draws attention to the tight constraints on amino acid positioning within the β3-strand of CTA1 for the formation of a functional enzymatic cleft. It might also be speculated from functional comparisons of the DTA and CTA1 active-site clefts that the catalytic role of the aromatic moiety within the DTA active-site cleft may be substituted in CTA1 by the tightly coordinated positioning of residues within the β3-strand of the NAD binding cleft.

In summary, it can be inferred from the limited-sequence homology within the enzymatically active regions of ADP-ribosylating proteins that different amino acids can perform a similar function when placed within the structural framework common to ADP-ribosylating proteins. Studies examining the functional interrelationship of residues in the β3-strand that form one side of the NAD binding cleft support that DT and CT maintain a similar mechanism of binding NAD but differ in their mechanism of NAD hydrolysis. While our studies focused on Tyr54 in DTA and Ser61 in CTA1 in the β3-strands in differentiating the activity of the respective toxins, the function of these residues is known to be coordinated with other residues in the active-site cleft. The specific functional counterpart of Tyr54 in DT is His21 (*2*) and that of Ser61 in CT is Arg7 (*34*). The inability of a His21-to-arginine mutation to restore enzymatic function of the Y54S DTA mutant (unpublished observation), coupled with the restricted sequence flexibility allowed the CTA1 β3-strand for function, however supports that the coordinated function of Tyr54 in DT and Ser61 in CT has co-evolved with multiple residues within their respective NAD binding clefts.

ACKNOWLEDGMENT

We thank Drs. Timothy Vincent, Eileen McGuffie, and Joseph Dolan for their helpful comments during these studies.

REFERENCES

1. Sixma, T., Pronk, S., Kalk, K., Wartna, E., van Zanten, B., Witholt, B., and Hol, W. (1991) *Nature 351*, 371−377.
2. Bell, C. E., and Eisenberg, D. (1996) *Biochemistry 35*, 1137−1149.
3. van den Akker, F., Sarfaty, S., Twiddy, E. M., Connell, T. D., Holmes, R. K., and Hol, W. G. J. (1996) *Structure 4*, 665−678.
4. Li, M., Dyda, F., Benhar, I., Pastan, I., and Davies, D. R. (1996) *Proc. Natl. Acad. Sci. U.S.A. 93*, 6902−6906.
5. Domenighini, M., and Rappuoli, R. (1996) *Mol. Microbiol. 21*, 667−674.
6. Kulich, S. M., Yahr, T. L., Mende-Mueller, L. M., Barbieri, J. T., and Frank, D. W. (1994) *J. Biol. Chem. 269*, 10431−10437.
7. Liu, S., Kulich, S. M., and Barbieri, J. T. (1996) *Biochemistry 35*, 2754−2758.
8. Laemmli, U. K. (1970) *Nature (London) 227*, 680−685.
9. Price, S. R., Welsh, C. F., Haun, R. S., Stanley, S. J., Moss, J., and Vaughan, M. (1992) *J. Biol. Chem. 267*, 17766−17772.
10. Carroll, S. F., and Collier, R. J. (1988) *Methods Enzymol. 165*, 218−225.
11. Beattie, B. K., Prentice, G. A., and Merrill, A. R. (1996) *Biochemistry 35*, 15134−15142.
12. Kulich, S. M., Frank, D. W., and Barbieri, J. T. (1993) *Infect. Immun. 61*, 307−13.
13. Olson, J. C., McGuffie, E. M., and Frank, D. W. (1997) *Infect. Immun. 65*, 248−256.
14. Moss, J., Manganiello, V. C., and Vaughan, M. (1976) *Proc. Natl. Acad. Sci. U.S.A. 73*, 4424−4427.
15. Tsai, S.-C., Noda, M., Adamik, R., Chang, P. P., Chen, H.-C., Moss, J., and Vaughan, M. (1988) *J. Biol. Chem. 263*, 1768−1772.
16. Towbin, H., Staehelin, T., and Gordon, J. (1979) *Proc. Natl. Acad. Sci. U.S.A. 76*, 4350−4354.
17. Olson, J. C. (1993) *J. Bacteriol. 175*, 898−901.
18. Wilson, B. A., Reich, K. A., Weinstein, B. R., and Collier, R. J. (1990) *Biochemistry 29*, 8643−8651.
19. Carroll, S. F., and Collier, R. J. (1984) *Proc. Natl. Acad. Sci. U.S.A. 81*, 3307−3311.
20. Harford, S., Dykes, C. W., Hobden, A. N., Read, H. J., and Halliday, I. J. (1989) *Eur. J. Biochem. 183*, 311−316.
21. Magagnoli, C., Manetti, R., Fontana, M. R., Giannelli, V., Giuliani, M. M., Rappuoli, R., and Pizza, M. (1997) *Infect. Immun. 64*, 5434−5438.
22. Moss, J., and Vaughan, M. (1977) *J. Biol. Chem. 252*, 2455−2457.
23. Coburn, J., Wyatt, R. T., Iglewski, B. H., and Gill, D. M. (1989) *J. Biol. Chem. 264*, 9004−9008.
24. Gill, D. M., and Meren, R. (1978) *Proc. Natl. Acad. Sci. U.S.A. 75*, 3050−3054.
25. Moss, J., and Vaughan, M. (1988) *Adv. Enzymol. Relat. Areas Mol. Biol. 61*, 303−379.
26. Scott, D. L., Zhang, R.-G., and Westbrook, E. M. (1996) *The Cholera Toxin Family of Enterotoxins*, R. G. Landes Co., Austin, TX.
27. Kahn, R. A., and Gillman, A. G. (1984) *J. Biol. Chem. 259*, 6228−6234.
28. Fu, H., Coburn, J., and Collier, R. J. (1993) *Proc. Natl. Acad. Sci. U.S.A. 90*, 2320−2324.
29. Galloway, T. S., and van Heyningen, S. (1987) *Biochemistry 26*, 225−230.
30. Wilson, B. A., Blanke, S. R., Reich, K. A., and Collier, R. J. (1994) *J. Biol. Chem. 269*, 23296−23301.
31. Lukac, M., and Collier, R. J. (1988) *Biochemistry 27*, 7629−7632.
32. Bell, C. E., Yeates, T. O., and Eisenberg, D. (1997) *Protein Sci. 6*, 2084−2096.
33. Pizza, M., Domenighini, M., Hol, W., Giannelli, V., Fontana, M. R., Giuliani, M. M., Magagnoli, C., Peppoloni, S., Manetti, R., and Rappuoli, R. (1994) *Mol. Microbiol. 14*, 51−60.
34. Sixma, T. K., Kalk, K. H., van Zanten, B. A. M., Dauter, Z., Kingma, J., Witholt, B., and Hol, W. G. J. (1993) *J. Mol. Biol. 230*, 890−918.
35. Ceiplak, W., Jr., Mead, D. J., Messer, R. J., and Grant, C. C. R. (1995) *J. Biol. Chem. 270*, 30545−30550.
36. Kabsch, W. (1978) *Acta Crystallogr. A 34*, 827−828.
37. Koch-Nolte, F., Peterson, D., Balasubramanian, S., Haag, F., Kahlke, D., Willer, T., Kastelein, R., Bazan, F., and Thiele, H.-G. (1996) *J. Biol. Chem. 271*, 7686−7693.

BI992856Q